Inorganic Chemistry

Article

pubs.acs.org/IC

Synthesis, Crystal Structures, and Magnetic Properties of Cyanide-Bridged $W^{V}Mn^{III}$ Anionic Coordination Polymers Containing Divalent Cationic Moieties: Slow Magnetic Relaxations and Spin Crossover Phenomenon

Jung Hee Yoon,[†] Kwang Soo Lim,[†] Dae Won Ryu,[†] Woo Ram Lee,[†] Sung Won Yoon,[‡] Byoung Jin Suh,[‡] and Chang Seop Hong*[,†]

[†]Department of Chemistry (BK21), Korea University, Seoul 136-713, Korea

[‡]Department of Physics, The Catholic University of Korea, Buchon 420-743, Korea

Supporting Information

ABSTRACT: Two trimetallic coordination complexes were prepared by self-assembly of $[W(CN)_8]^{3-}$ and the Mn(III) Schiff base followed by the addition of a Zn(II) or Fe(II) cationic unit. The octacyanotungstate connects neighboring Mn(III) centers to form a one-dimensional chain. The anionic chain requires cationic units of Zn(II) or Fe(II) to maintain charge balance in the structure. The Zn-containing complex shows ferrimagnetic behavior originating from the antiparallel alignment of W(V) and Mn(III) spins within the chain, which leads to slow magnetic relaxation at low temperatures. For the Fe(II)-containing compound, Fe(II) moieties are integrated into the ferrimagnetic chains, altering their spin states depending on the temperature. It appears that the coexistence of high- and low-spin states in the low temperature regime is responsible for the slower and faster relaxations of the magnetization.

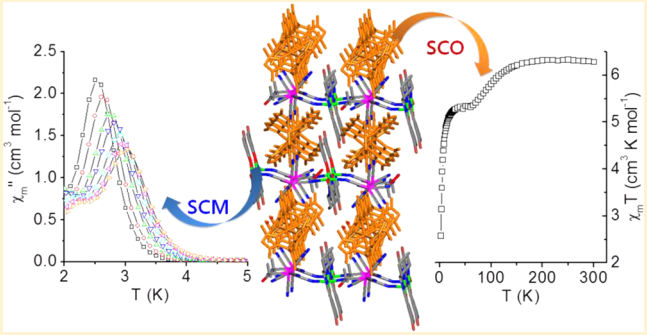

INTRODUCTION

The introduction of multifunctionalities in molecule-based magnetic materials is receiving a lot of interest in recent times. From a coordination chemistry point of view, these multifunctionalities are introduced by taking advantage of the intrinsic nature of metal constituents and bridging units. Using this approach, some secondary functionalities can be achieved, which include conductivity, chirality, photo- and piezoswitching behaviors, porosity, and multiferroics.[1,2]

In addition to molecular magnets showing long-range magnetic order, the chemical design and synthesis of nanoscale objects are appealing for fundamental and application aspects. In this vein, single-molecule magnets (SMMs) and single-chain magnets (SCMs) have been studied extensively to facilitate the in-depth understanding of magnet-like dynamics at a molecular or one-dimensional level.[3−5] Specifically, it is now understood that SCMs are controlled by critical elements of anisotropic metal constituents and intrachain magnetic couplings that are dominant over interchain ones.[5] Therefore, it is imperative that magnetic chains are separated as much as possible to minimize interchain magnetic interactions. Magnetic isolation to create slow magnetic relaxation can be achieved by incorporating bulky ligands or diamagnetic moieties between the chains. Keeping these key strategies in mind, suitable metal ions and ligands can be selected to provide dual functionalities in a single compound. Indeed, examples of some SCM materials that have additional properties such as chirality,[6] microporosity,[7] and photoswitching[8] have been shown.

Molecular switchable materials are attracting attention in the field of molecular magnetism owing to their promise for use as switches, sensors, and memory devices.[9] The characteristic of switching between the low-spin and high-spin states found in an octahedral Fe(II) ion is sensitive to external stimuli and triggered by temperature, pressure, light, or solvent.[10] Since the spin crossover (SCO) phenomenon occurs in a monomeric complex, formulating a material with both SCO and other properties is rather straightforward. In fact, SCO-based materials have reportedly displayed secondary properties such as spin glasses,[11] chirality,[12] conductivity,[13] magnetic order,[14] SMM,[15] and sorption.[16]

Recently, we demonstrated that the SCO property coexists with SCM behavior in ferromagnetic $Mo^{V}Mn^{III}$ chains containing Fe^{II} moieties.[17] However, examples of substances possessing both SCM and SCO are still rare, and further exploration is needed to examine the underlying magnetic features. Herein, we report on the synthesis, structures, and magnetic properties of 1D chains $[W(CN)_8Mn(5\text{-Brsalcy})]$-

Received: June 24, 2014
Published: September 23, 2014

Scheme 1. Chemical Structures of Ligands Used

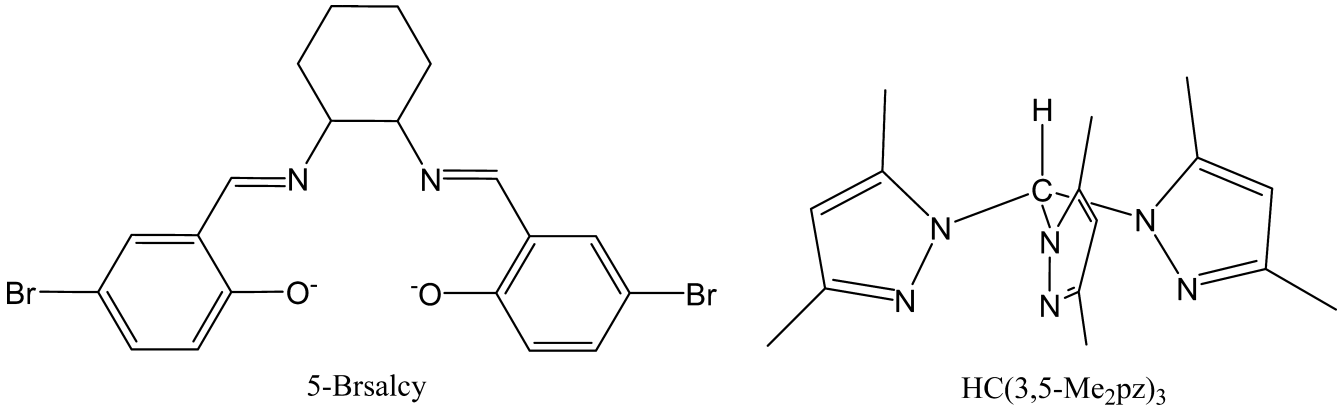

$\{M[HC(3,5\text{-}Me_2pz)_3]_2\}\cdot x(solvents)$ [M = Zn (**1**) and Fe (**2**); 5-Brsalcy = *N*,*N*′-(*trans*-1,2-cyclohexanediylethylene)bis(5-bromosalicylideneiminato) dianion]. Scheme 1. Complex **1** shows slow magnetic relaxation from well-isolated antiferromagnetic $W^{V}Mn^{III}$ chains, while the SCM trait accompanies the SCO phenomenon in **2**.

EXPERIMENTAL SECTION

General Procedures and Materials. All chemicals and solvents in the synthesis were reagent grade and used as received. $Cs_3W(CN)_8\cdot 2H_2O$[18] and $Fe[HC(3,5\text{-}Me_2pz)_3]_2(BF_4)_2$[19−21] were prepared according to the procedure given in the literature. The perchlorate salts of metal compounds with organic ligands are potentially explosive, and cyanides are toxic. Therefore, only small amounts of the material should be handled, and due caution should be exercised.

$\{Zn[HC(3,5\text{-}Me_2pz)_3]_2\}(NO_3)_2$. This was synthesized according to a modified procedure.[22] $Zn(NO_3)_2\cdot 6H_2O$ (0.1 mmol) was added to a THF (20 mL) solution of $HC(3,5\text{-}Me_2pz)_3$ (0.2 mmol). After the solution was stirred for 1 d, the resulting mixture was diffused with ether (150 mL) for 1 d. The white powder that formed was filtered off, washed with ether, and dried in air. Yield: 34%. Anal. Calcd for $C_{32}H_{44}N_{14}O_6Zn$: C, 48.89; H, 5.64; N, 24.94. Found: C, 49.00; H, 5.24; N, 24.72.

*$[W(CN)_8Mn(5\text{-}Brsalcy)]\{Zn[HC(3,5\text{-}Me_2pz)_3]_2\}$ (**1**).* $Cs_3W(CN)_8\cdot 2H_2O$ (0.05 mmol) solid and $Zn[HC(3,5\text{-}Me_2pz)_3]_2(NO_3)_2$ (0.05 mmol) solid were added to a solution of $[Mn(5\text{-}Brsalcy)(H_2O)]ClO_4$ (0.05 mmol) in mixed MeOH/acetone/H_2O solvent (10:10:3, v/v). After the solution was stirred for 1 min, the reaction solution was filtered and slowly evaporated in the dark at room temperature for 2 d. The red crystals that formed were filtered, washed with MeOH/acetone, and dried in air. Yield: 27%. Anal. Calcd for $C_{63}H_{68}Br_2N_{22}O_3MnZnW$ (**1**·acetone): C, 45.99; H, 4.17; N, 18.73. Found: C, 46.55; H, 4.12; N, 19.25.

*$[W(CN)_8Mn(5\text{-}Brsalcy)]\{Fe[HC(3,5\text{-}Me_2pz)_3]_2\}\cdot 2isopropanol\cdot H_2O$ (**2**).* $Cs_3W(CN)_8\cdot 2H_2O$ (0.05 mmol) solid and $Fe[HC(3,5\text{-}Me_2pz)_3]_2(BF_4)_2$ (0.05 mmol) solid were added to a solution of $[Mn(5\text{-}Brsalcy)(H_2O)]ClO_4$ (0.05 mmol) in mixed MeOH/MeCN/H_2O solvent (5:5:1, v/v). After the solution was stirred for 1 min, the resulting mixture was filtered and slowly evaporated in the dark at room temperature for 8 d. The red crystals that formed were immersed in isopropanol for 7 d. The crystals were filtered, washed with isopropanol, and dried in air for 2 h. Anal. Calcd for $C_{66}H_{80}Br_2FeMnN_{22}O_5W$: C, 46.20; H, 4.70; N, 17.96. Found: C, 45.86; H, 4.37; N, 17.72.

Physical Measurements. Elemental analyses for C, H, and N were performed at the Elemental Analysis Service Center of Sogang University. Infrared spectra were obtained from KBr pellets with a Bomen MB-104 spectrometer. Magnetic susceptibilities for **1** and **2** were determined using a Quantum Design SQUID susceptometer (dc) in the Seoul Branch of Korea Basic Science Institute (KBSI) and PPMS magnetometer (ac). Magnetic data were calibrated for the sample holder, and the magnitude of diamagnetism was estimated from Pascal's constants.

Crystallographic Structure Determination. X-ray data for **1** and **2** were collected on a Bruker SMART APEXII diffractometer equipped with graphite monochromated Mo Kα radiation (λ = 0.710 73 Å). The preliminary orientation matrix and cell parameters were determined from three sets of ω scans at different starting angles. Data frames were obtained at scan intervals of 0.5° with an exposure time of 10 s per frame. The reflection data were corrected for Lorentz and polarization factors. Absorption corrections were carried out using SADABS.[23] The structures were solved by direct methods and refined by full-matrix least-squares analysis using anisotropic thermal parameters for non-hydrogen atoms with the SHELXTL program.[24] All hydrogen atoms except for hydrogens bound to water molecules were calculated at idealized positions and refined with the riding models. Crystal data for **1**·MeOH·$5H_2O$: M_r = 1741.46, triclinic, space group $P\bar{1}$, a = 10.8160(6) Å, b = 13.8608(8) Å, c = 24.5131(15) Å, α = 89.373(2)°, β = 89.037(2)°, γ = 84.840(2)°, V = 3659.4(4) Å^3, Z = 2, D_{calc} = 1.580 g cm^{-3}, μ = 3.223 mm^{-1}, T = 130(2) K, 77 003 reflections collected, 15 718 unique (R_{int} = 0.0236), R1 = 0.0257, wR2 = 0.0681 [$I > 2\sigma(I)$]. Crystal data for **2**: M_r = 1655.89, triclinic, space group $P\bar{1}$, a = 10.7016(2) Å, b = 14.1793(3) Å, c = 24.4382(6) Å, α = 88.794(1)°, β = 87.291(1)°, γ = 82.459(1)°, V = 3671.69(14) Å^3, Z = 2, D_{calc} = 1.498 g cm^{-3}, μ = 3.074 mm^{-1}, T = 100(2) K, 43 345 reflections collected, 16 791 unique (R_{int} = 0.0383), R1 = 0.0555, wR2 = 0.1372 [$I > 2\sigma(I)$].

RESULTS AND DISCUSSION

Description of Structures. The crystal systems for both complexes were the same, and their space group was $P\bar{1}$. The data collection for **1** and **2** was carried out at 130 and 100 K, respectively. The crystal structures of **1** and **2** are depicted in Figure 1 and Supporting Information Figure S1. To determine the exact geometry around W, we performed a continuous shape measures (CShM) analysis (Table 1).[25] The S_X (X = SAPR, DD, BTP) values against the ideal symmetry of a square antiprism (SAPR, D_{4d}), dodecahedron (DD, D_{2d}), and bicapped trigonal prism (BTP, C_{2v}) clearly indicated that the W ion belonged to a distorted DD. The average W−C distances were identical: 2.17(1) Å for both **1** and **2**. The W−C−N angles were almost linear, ranging from 175.9° to 179.1° for **1** and 176.4° to 179.9° for **2**. For Mn coordination, the Mn atom adopted a distorted octahedral geometry consisting of four short equatorial (=eq) N(O) atoms [av Mn−$N(O)_{eq}$ distance = 1.93(7) Å for **1** and 1.94(6) Å for **2**] from 5-Brsalcy and two axial (=ax) N atoms [av Mn−N_{ax} = 2.348(9) Å for **1** and 2.309(9)Å for **2**] from the cyanide bridges. Jahn−Teller elongation is typical for high-spin Mn(III) ions in an octahedral environment. Another important internal parameter that affects

dx.doi.org/10.1021/ic501506s | Inorg. Chem. 2014, 53, 10437−10442

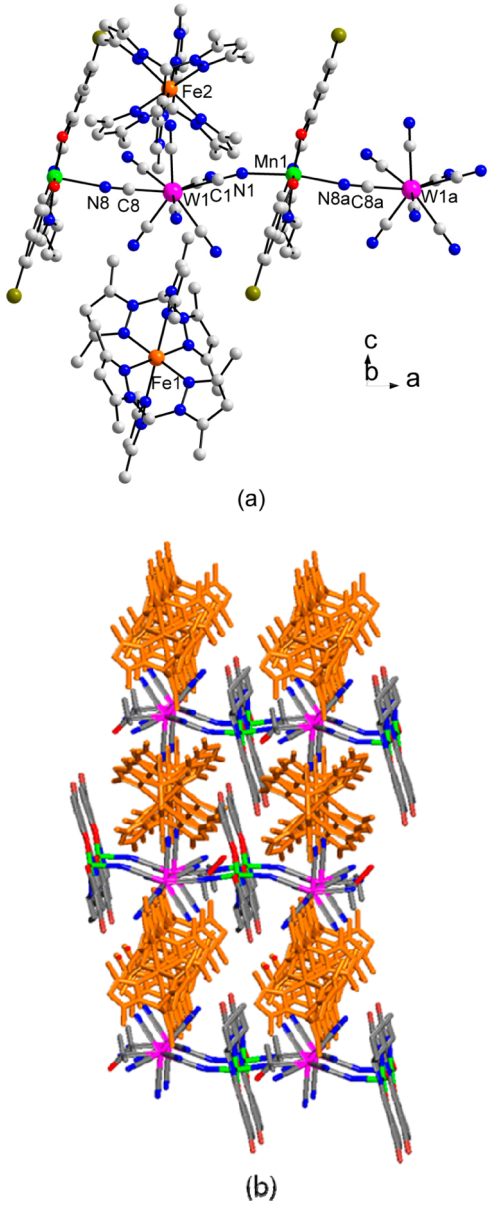

Figure 1. (a) Molecular view of **2**. Symmetry code: $a = 1 + x, y, z$. (b) Extended structure showing 1D chains along the *a*-axis and Fe moieties (orange) located between the chains.

magnetic interactions is the Mn−N−C angle along the bridging route, Mn1−N1−C1 = 159.8(2)°, Mn1−N8a−C8a = 167.5(3)° ($a = 1 + x, y, z$) for **1**, and Mn1−N1−C1 = 158.8(5)°, Mn1−N8a−C8a = 162.0(6)° for **2**. The octacyanotungstate(V) precursor acted as a bridge to the Mn(III) ions, leading to the formation of a one-dimensional bimetallic anionic chain. Within the chain, the distances between adjacent metal ions were 5.5700(3) Å for W1−Mn1 and 5.6395(1) Å for Mn1−W1a (**1**), and 5.5261(1) Å for W1−Mn1 and 5.5528(1) Å for Mn1−W1a (**2**).

The cationic counterpart of $\{M[HC(3,5\text{-}Me_2pz)_3]_2\}^{2+}$ (M = Zn^{2+} and Fe^{2+}) was incorporated into the anionic chain structure to maintain charge balance. For M = Fe, the Fe−N bond lengths were in the range 2.115−2.208 Å, which fall into the usual scope of a high-spin divalent state, indicating that a high-spin configuration is predominant at 100 K.[26] The chains were well separated by the inclusion of the cationic moieties located between them. The shortest interchain Mn−Mn distances were 10.672 Å for **1** and 10.702 Å for **2** (Supporting Information Figures S2 and S3). On the other hand, the Fe atoms were well-insulated from each other because of the presence of bulky Schiff base ligands, and the Fe−Fe distance in **2** was 10.702 Å. The $W^{V}Mn^{III}$ anionic chain had multiple weak intermolecular contacts with the cationic mononuclear Fe^{II} complexes through the N atoms of unbound cyanides and 3,5-Me_2pz ligands (Figure 2 and Supporting Information Figure S4). The cyanide groups also formed hydrogen bonds with water and isopropanol molecules.

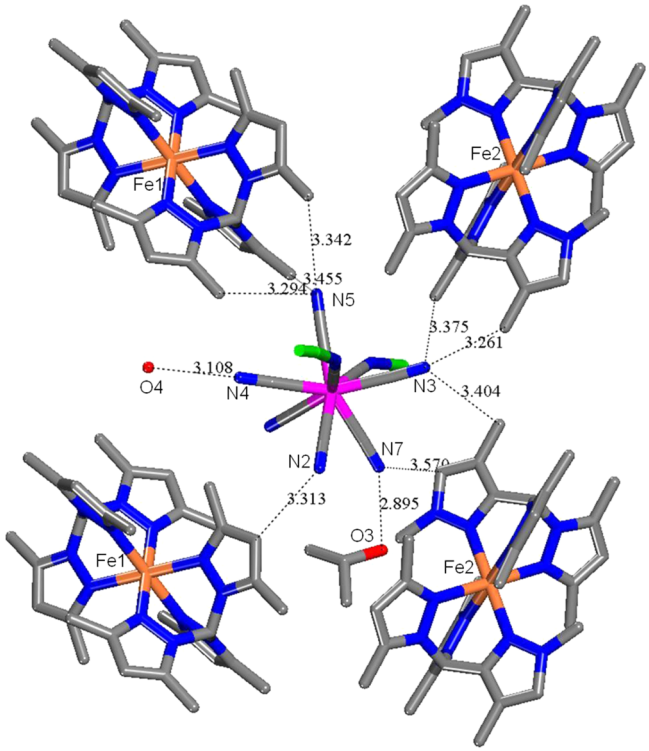

Figure 2. Intermolecular contacts among the chain, Fe moieties, and solvent molecules in **2**.

Table 1. Results of the Continuous Shape Measure Analysis[a]

		shape measures (S_X) relative to				φ	
complex	metal center	SAPR	DD	BTP	Δ(SAPR, DD)	(SAPR > DD)	(DD > SAPR)
1	W1	3.00931	0.34980	2.77350	0.379	102.8%	34.9%
2	W1	1.69982	0.42980	2.54066	0.228	77.1%	38.7%

[a] S_{DD} is the shape measure relative to the dodecahedron, S_{SAPR} the shape measure relative to the square antiprism, S_{BTP} the shape measure relative to the bicapped trigonal prism, Δ(SAPR, DD) indicates the deviation from the DD-SAPR interconversion path, and φ(SAPR > DD) and φ(DD > SAPR) the generalized interconversion coordinates. The sum φ(SAPR > DD) + φ(DD > SAPR) is larger than 100% because of the nonzero value of Δ(SAPR, DD).

dx.doi.org/10.1021/ic501506s | *Inorg. Chem.* 2014, 53, 10437−10442

Static Magnetic Properties. The magnetic susceptibility data for **1** was collected at 1 kG as a function of temperature (Figure 3a). The $\chi_m T$ value at 300 K is equal to 3.40 cm^3 K

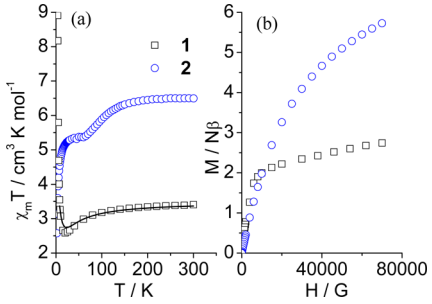

Figure 3. Plots of (a) $\chi_m T$ versus T at 1000 G and (b) M versus H per WMnFe at 2 K for **1** and **2**.

mol^{-1}, which is consistent with that of noncoupled W(V) and Mn(III) ions (3.38 cm^3 K mol^{-1}). The steady decrease in $\chi_m T$ is associated with the antiferromagnetic arrangement between the heterospins. The sharp rise after a minimum in $\chi_m T$ is due to the enhanced correlation of the resultant spins along the chain, which is diagnostic of a ferrimagnetic consequence of S_{Mn} and S_W within a chain. To evaluate the magnetic exchange coupling constant, we employed an infinite chain model with the spin Hamiltonian $\mathbf{H} = -2J\Sigma_i(\mathbf{S}_{Mni}\cdot\mathbf{S}_{Wi} + \mathbf{S}_{Mni}\mathbf{S}_{Wi+1})$, derived by Seiden with the consideration of an interchain term (zJ').[27,28] A best fit of the data with the equation resulted in g = 2.04(2), J = −12(2) cm^{-1}, and zJ' = −0.2(1) cm^{-1}. The negative J parameter indicates the operation of intrachain antiferromagnetic couplings between magnetic spins mediated by the cyanide bridge. Weak antiferromagnetic interactions exist between neighboring chains, as indicated by the zJ' term.

Compared to the magnetic trait of **1**, the magnetic trend of **2** is rather complicated. At 300 K, the $\chi_m T$ value of 6.50 cm^3 K mol^{-1} is close to the theoretical value (6.38 cm^3 K mol^{-1}) expected from noninteracting W^V (S_W = $^1/_2$), Mn^{III} (S_{Mn} = 2), and high-spin Fe^{II} (S_{Fe}^{hs} = 2) spins. As the temperature decreases, the $\chi_m T$ product undergoes a gradual reduction followed by a more pronounced decrease below 125 K, which continues until 65 K. This distinct feature of **2** is different from the magnetic behavior of **1** over an identical temperature range, where a gradual decay in $\chi_m T$ is observed. Such disparity originates from the existence of a paramagnetic high-spin Fe(II) ion in **2** because **1** contains the diamagnetic Zn(II) ion. Since the SCO phenomenon was observed for the $\{Fe[HC(3,5\text{-}Me_2pz)_3]_2\}^{2+}$ complexes in which the properties are sensitive to the variation in Fe(II) geometries affected by crystalline forms and anion types, the appreciable reduction in $\chi_m T$ clearly originates from the magnetic contribution of the Fe(II) fragment.[19−22] Since the Fe(II) complexes between the chains are far away from each other, it is clear that the cooperativity over the lattice is expected to be low. The transition from a high-spin to low-spin configuration is incomplete, which is probably due to the fact that the field strength for the low-spin state is insufficient.[29]

Moreover, the magnetic trend should be influenced by intrachain exchange interactions. To assess the nature of the magnetic exchange, we performed DFT calculations on the $W(CN)_8^{3-}$ fragment. The calculations demonstrated that the spin density of the W $d_{x^2-y^2}$ type orbital is delocalized over the N $p\pi$ orbital of the cyanide ligands (Figure 4). The N $p\pi$ orbital of

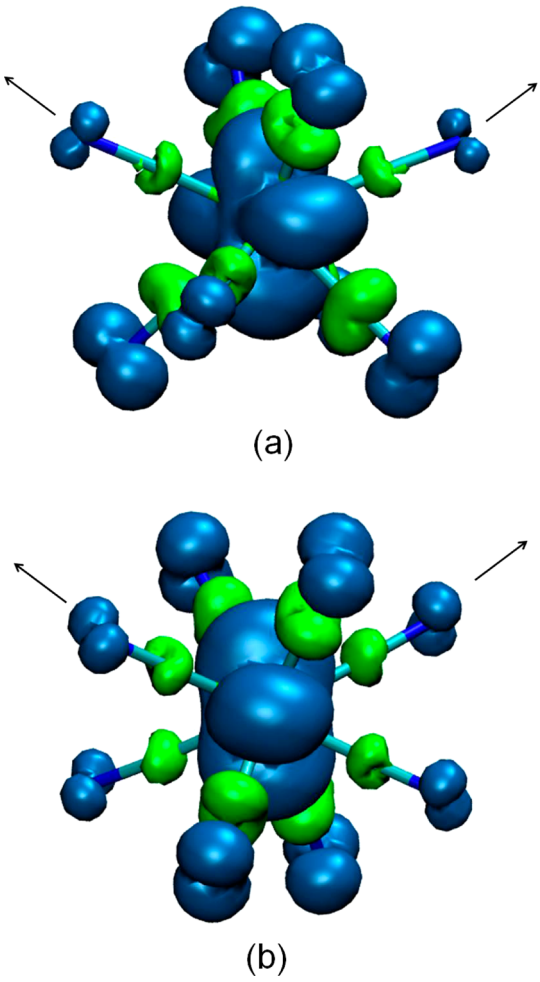

Figure 4. Spin density of the $[W(CN)_8]^{3-}$ precursor for (a) **1** and (b) **2** with a W $d_{x^2-y^2}$ type magnetic orbital, derived from B3LYP DFT calculations performed with Gaussian 09. The basis set for all atoms is LANL2DZ. For **1**, NBO analysis shows that spin density is 0.82928 on W, 0.01915 and 0.02265 on bridging N atoms, and 0.03662−0.08347 on the other free N atoms. For **2**, NBO analysis shows that spin density is 0.83479 on W, 0.02796 and 0.02897 on bridging N atoms, and 0.03096−0.08431 on the other free N atoms.

the bridging cyanide overlaps the Mn d_{z^2} orbital oriented toward the axial direction. Given that the axial elongation is pronounced for **1** and **2**, the Mn d_{z^2} orbital serves as a dominant magnetic contributor. In this situation, the magnetic nature can be determined by the Mn−N−C angle in the bridging pathway. Ferromagnetic coupling emerged owing to the strict orthogonality at the Mn−N−C angle of 180°, and antiferromagnetic coupling occurred when the angle decreased below the crossover point.[30] Since the Mn−N−C angle (160.4°) of **2** was slightly smaller than that (163.7°) of **1**, antiferromagnetic interaction should be favored in **2** on the basis of the above orbital consideration. Hence, the SCO behavior from the Fe(II) moieties and intrachain antiferromagnetic interactions between W(V) and Mn(III) spins were responsible for the decay in $\chi_m T$ for **2**.

To evaluate the spin state at low temperature, we measured the field dependence of the magnetization (Figure 3b). The magnetization value of 2.74 Nβ at 7 T for **1** was slightly smaller than the ferrimagnetic consequence of **2**, (S_{Mn} − S_W) = 3 Nβ, because of the magnetic anisotropy. The magnetization curve for **2** increased more slowly in the low field and reached 5.73

dx.doi.org/10.1021/ic501506s | Inorg. Chem. 2014, 53, 10437−10442

Nβ at 7 T. The difference between the magnetization values at 7 T for **1** and **2** corresponded to 2.99 Nβ, which is related to the Fe(II) spin. With respect to the theoretical saturation value of 4 Nβ for a high-spin Fe(II) ion, assuming $g = 2$, the fraction of the high-spin configuration was roughly estimated to be 75% at 2 K. The precise fraction of the high-spin to low-spin configuration needs to be confirmed by Mössbauer spectroscopy although the $\chi_m T$ curve suggests the presence of SCO behavior.

Dynamic Magnetic Properties. The spin dynamics of **1** and **2** were investigated using ac magnetic susceptibility data. A weak frequency dependence was observed in **1**, indicating the presence of slow magnetic relaxation (Supporting Information Figures S5 and S6). In contrast, clear slow relaxations were observed in **2**. In the $\chi_{ac}(T)$ plots of **2**, the main peaks in the high-temperature (T) region ($T > 2.4$ K) are followed by weak signals in the low-T range 2.0−2.4 K (Figure 5a and Supporting Information Figure S7). To probe the relaxation process ($T > 2.4$ K) of **2**, we inspected the peak corresponding to the maxima in the $\chi_m''(T)$ curve; this peak moves toward higher temperature as f increases. The formula of $\phi = \Delta T_p/[T_p \Delta(\log f)]$ was utilized to estimate the value of ϕ as being ~0.14, which exceeds the conventional range for spin glasses and agrees well with that of a superparamagnet.[31] The obtained value suggests the presence of slow magnetic relaxation typical for a SCM. Similarly, two slow relaxations are also evident in the $\chi_m''(f)$ plots at temperatures ranging from 2.0 to 2.4 K, while only a single relaxation is present at $T > 2.4$ K (Figure 5b and Supporting Information Figure S8). We employed a generalized Debye model to fit the $\chi_m''(f)$ data. The extracted relaxation times were inserted into the Arrhenius equation, $\tau = \tau_0 \exp(\Delta_\tau/kT)$, where $\tau = 1/2\pi f$, leading to the parameters $\tau_0 = 2.5 \times 10^{-8}$ s and $\Delta_\tau/k = 16.7$ K for the faster relaxation (FR) and $\tau_0 = 6.7 \times 10^{-11}$ s and $\Delta_\tau/k = 39.6$ K for the slower relaxation (SR). In the Cole−Cole diagrams, the two relaxations are also visible (Supporting Information Figure S9). The fitted α terms with a generalized Debye model are less than 0.36 for SR and 0.41 for FR. The results suggest the distribution of single relaxation processes. One possible scenario for the two unique relaxations is the coexistence of low-spin and high-spin Fe(II) configurations in the low-temperature region. The high-spin Fe(II) ions could couple in an antiparallel manner with noncompensated spins in adjacent chains, resulting in FR. In contrast, SR may originate from the region where low-spin Fe(II) ions are present.

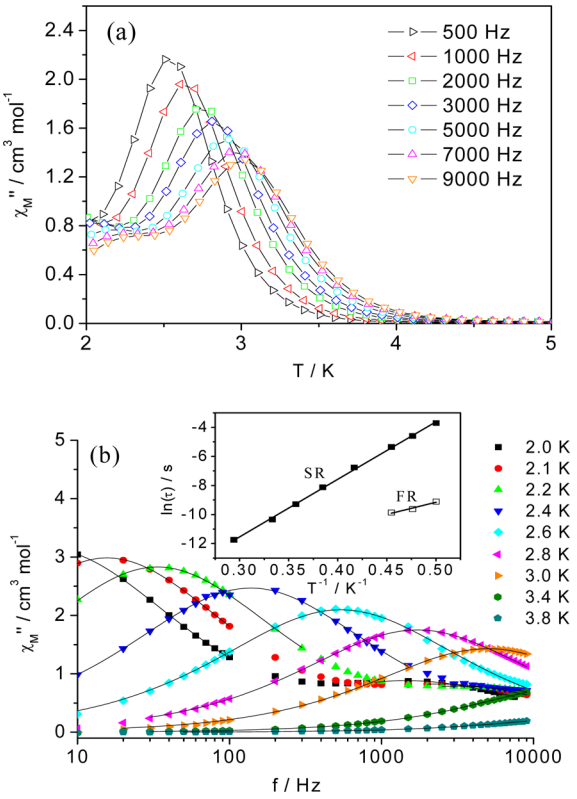

Figure 5. Plots of (a) χ_m'' versus T and (b) χ_m'' versus f for **2** at zero dc field and an ac field of 5 G. The lines in part b are the fits with the generalized Debye model. The inset shows Arrhenius plots.

The correlation length (ξ) in the Ising chain can be expressed using the following equation: $\chi T = C_{eff} \exp(\Delta_\xi/kT)$, where Δ_ξ is the barrier required to construct a domain wall within the chain.[32] To calculate the activation energy for **2**, we plotted $\ln(\chi_m' T)$ as a function of $1/T$ (Supporting Information Figure S10). Using the slope of the straight line, the barrier energy (Δ_ξ) was estimated to be 0.63 K (0.44 cm^{-1}), which corresponds to the J value of 0.11 cm^{-1} based on $\Delta_\xi = 4JS_1S_2$.[33] We conjectured that the J values for **1** and **2** are similar because of similar structural parameters relevant to the magnetic pathways in the W(V)Mn(III) chain. With this assumption, the rough estimate for the J parameter of **2** was much smaller than that obtained from the magnetic susceptibility data for **1**, which could be due to a deviation from an Ising chain system and/or additional contribution from antiferromagnetic interactions between the Fe(II) spins and 1D chains at low temperatures.

CONCLUSIONS

We prepared trimetallic systems consisting of $W^{V}Mn^{III}$ anionic chains and $\{M[HC(3,5\text{-}Me_2pz)_3]_2\}^{2+}$ [M = Zn (**1**) and Fe (**2**)] cations. The well-separated antiferromagnetic chains result in slow magnetic relaxations in **1** and the coexistence of SCM and SCO behaviors in **2**. It appears that the faster and slower relaxations in **2** are associated with the presence of high-spin and low-spin states of Fe(II). Light-irradiation experiments will be required to investigate effects on SCM behavior by light-induced excited spin-state trapping.

ASSOCIATED CONTENT

Supporting Information

X-ray crystallographic files in CIF format. Additional structural and magnetic data for the complexes. This material is available free of charge via the Internet at http://pubs.acs.org.

AUTHOR INFORMATION

Corresponding Author

*E-mail: cshong@korea.ac.kr.

Notes

The authors declare no competing financial interest.

ACKNOWLEDGMENTS

This work was supported by the Korea CCS R&D Center (KCRC) grant funded by the Korea government [The Ministry of Science, ICT & Future Planning (MSIP)] (NRF-2014M1A8A1049253), by Basic Science Research Program

(NRF-2012R1A1A2007141), and by Priority Research Centers Program (NRF20100020209).

REFERENCES

(1) Clemente-León, M.; Coronado, E.; Martí-Gastaldo, C.; Romero, F. M. *Chem. Soc. Rev.* **2011**, *40*, 473−497.
(2) Train, C.; Gruselle, M.; Verdaguer, M. *Chem. Soc. Rev.* **2011**, *40*, 3297−3312.
(3) Woodruff, D. N.; Winpenny, R. E.; Layfield, R. A. *Chem. Rev.* **2013**, *113*, 5110−5148.
(4) Layfield, R. A. *Organometallics* **2014**, *33*, 1084−1099.
(5) Zhang, W.-X.; Ishikawa, R.; Breedlove, B.; Yamashita, M. *RSC Adv.* **2013**, *3*, 3772−3798.
(6) Pardo, E.; Train, C.; Lescouëzec, R.; Journaux, Y.; Pasán, J.; Ruiz-Pérez, C.; Delgado, F. S.; Ruiz-Garcia, R.; Lloret, F.; Paulsen, C. *Chem. Commun.* **2010**, *46*, 2322−2324.
(7) Ouellette, W.; Prosvirin, A. V.; Whitenack, K.; Dunbar, K. R.; Zubieta, J. *Angew. Chem., Int. Ed.* **2009**, *48*, 2140−2143.
(8) Liu, T.; Zhang, Y.-J.; Kanegawa, S.; Sato, O. *J. Am. Chem. Soc.* **2010**, *132*, 8250−8251.
(9) Bousseksou, A.; Molnár, G.; Salmon, L.; Nicolazzi, W. *Chem. Soc. Rev.* **2011**, *40*, 3313−3335.
(10) Nihei, M.; Tahira, H.; Takahashi, N.; Otake, Y.; Yamamura, Y.; Saito, K.; Oshio, H. *J. Am. Chem. Soc.* **2010**, *132*, 3553−3560.
(11) Neves, A. I. S.; Dias, J. C.; Vieira, B. J. C.; Santos, I. C.; Branco, M. B. C.; Pereira, L. C. J.; Waerenborgh, J. C.; Almeida, M.; Belo, D.; Gama, V. d. *CrystEngComm* **2009**, *11*, 2160−2168.
(12) Sunatsuki, Y.; Ikuta, Y.; Matsumoto, N.; Ohta, H.; Kojima, M.; Iijima, S.; Hayami, S.; Maeda, Y.; Kaizaki, S.; Dahan, F.; Tuchagues, J. P. *Angew. Chem., Int. Ed.* **2003**, *42*, 1614−1618.
(13) Takahashi, K.; Cui, H.-B.; Okano, Y.; Kobayashi, H.; Mori, H.; Tajima, H.; Einaga, Y.; Sato, O. *J. Am. Chem. Soc.* **2008**, *130*, 6688−6689.
(14) Arai, M.; Kosaka, W.; Matsuda, T.; Ohkoshi, S. *Angew. Chem., Int. Ed.* **2008**, *47*, 6885−6887.
(15) Ababei, R.; Pichon, C.; Roubeau, O.; Li, Y. G.; Bréfuel, N.; Buisson, L.; Guionneau, P.; Mathonière, C.; Clérac, R. *J. Am. Chem. Soc.* **2013**, *135*, 14840−14853.
(16) Coronado, E.; Giménez-Marqués, M.; Mínguez Espallargas, G.; Rey, F.; Vitórica-Yrezábal, I. J. *J. Am. Chem. Soc.* **2013**, *135*, 15986−15989.
(17) Yoon, J. H.; Ryu, D. W.; Choi, S. Y.; Kim, H. C.; Koh, E. K.; Tao, J.; Hong, C. S. *Chem. Commun.* **2011**, *47*, 10416−10418.
(18) Bok, L. D. C.; Leipoldt, J. G.; Basson, S. S. *Z. Anorg. Allg. Chem.* **1975**, *415*, 81−83.
(19) Reger, D. L.; Little, C. A. *Inorg. Chem.* **2001**, *40*, 2870−2874.
(20) Piquer, C.; Grandjean, F. *Inorg. Chem.* **2003**, *42*, 982−985.
(21) Reger, D. L.; Little, C. A.; Smith, M. D.; Rheingold, A. L.; Lam, K.-C.; Concolino, T. L.; Long, G. J.; Hermann, R. P.; Grandjean, F. *Eur. J. Inorg. Chem.* **2002**, 1190−1197.
(22) Reger, D. L.; Little, C. A. *Inorg. Chem.* **2001**, *40*, 1508−1520.
(23) Sheldrick, G. M. *SADABS, A Program for Area Detector Absorption Corrections*. University of Göttingen: Göttingen, Germany, 1994.
(24) Sheldrick, G. M. *SHELXTL, Version 5*; Bruker AXS: Madison, WI, 1995.
(25) Llunell, M.; Casanova, D.; Cirera, J.; Bofill, J. M.; Alemany, P.; Alvarez, A. *SHAPE, v1.1b*; Barcelona, 2005.
(26) Hauser, A. *Adv. Polym. Sci.* **2004**, *233*, 49−58.
(27) Seiden, J. *J. Phys., Lett.* **1983**, *44*, 947−952.
(28) Harris, T. D.; Coulon, C.; Clérac, R.; Long, J. R. *J. Am. Chem. Soc.* **2011**, *133*, 123−130.
(29) Gütlich, P.; Goodwin, H. A. *Top. Curr. Chem.* **2004**, *233*, 1−47.
(30) Lee, J. W.; Lim, K. S.; Ryu, D. W.; Koh, E. K.; Yoon, S. W.; Suh, B. J.; Hong, C. S. *Inorg. Chem.* **2013**, *52*, 8677−8684.
(31) Mydosh, J. A. *Spin Glasses: An Experimental Introduction*; Taylor & Francis: London, 1993.
(32) Bogani, L.; Vindigni, A.; Sessoli, R.; Gatteschi, D. *J. Mater. Chem.* **2008**, *18*, 4750−4758.
(33) Harris, T. D.; Bennett, M. V.; Clérac, R.; Long, J. R. *J. Am. Chem. Soc.* **2010**, *132*, 3980−3988.